Bioluminescent imaging of Ca^{2+} activity reveals spatiotemporal dynamics in glial networks of dark-adapted mouse retina

Cendra Agulhon[1], Jean-Claude Platel[3], Bogdan Kolomiets[5,6,7], Valérie Forster[5,6], Serge Picaud[5,6,7], Jacques Brocard[4], Philippe Faure[2] and Philippe Brulet[1]

[1] *Unité d'Embryologie Moléculaire, CNRS URA 2578, and* [2] *Unité de Neurobiologie Intégrative des Systémes Cholinergiques Institut Pasteur, 25–28 rue du Docteur Roux, 75724 Paris Cedex, France*
[3] *INSERM U704, Dynamique des Réseaux Neuronaux, Grenoble, F-38041, France*
[4] *INSERM U366, Laboratoire du Cytosquelette, Grenoble F-38054, France*
[5] *INSERM U592, Laboratoire de Physiopathologie Cellulaire et Moléculaire de la Rétine, Paris, France*
[6] *Université Pierre et Marie Curie-Paris 6, UMR S592, F-75012 Paris, France*
[7] *Fondation Ophtalmologique A. de Rothschild, F-75012 Paris, France*

Glial Ca^{2+} excitability plays a key role in reciprocal neuron–glia communication. In the retina, neuron–glia signalling is expected to be maximal in the dark, but the glial Ca^{2+} signal characteristics under such conditions have not been evaluated. To address this question, we used bioluminescence imaging to monitor spontaneous Ca^{2+} changes under dark conditions selectively in Müller cells, the principal retinal glial cells. By combining this imaging approach with network analysis, we demonstrate that activity in Müller cells is organized in networks of coactive cells, involving 2–16 cells located distantly and/or in clusters. We also report that spontaneous activity of small networks (2–6 Müller cells) repeat over time, sometimes in the same sequential order, revealing specific temporal dynamics. In addition, we show that networks of coactive glial cells are inhibited by TTX, indicating that ganglion and/or amacrine neuronal cells probably regulate Müller cell network properties. These results represent the first demonstration that spontaneous activity in adult Müller cells is patterned into correlated networks that display repeated sequences of coactivations over time. Furthermore, our bioluminescence technique provides a novel tool to study the dynamic characteristics of glial Ca^{2+} events in the retina under dark conditions, which should greatly facilitate future investigations of retinal dark-adaptive processes.

(Received 1 May 2007; accepted after revision 6 July 2007; first published online 12 July 2007)
Corresponding author C. Agulhon: Department of Pharmacology, 1004 Mary Ellen Jones Building, University of North Carolina at Chapel Hill, Chapel Hill, NC 27599-7365, USA. Email: cendra_agulhon@med.unc.edu

Although astrocytes have long been assigned a neuron-supportive role, considerable recent evidence suggests that they directly participate in information processing (Haydon, 2001; Fields & Stevens-Graham, 2002; Perea & Araque, 2005*a*,*b*; Volterra & Meldolesi, 2005). Astrocytes can respond to synaptically released neurotransmitters and modulate neuronal excitability by releasing neuroactive molecules, including adenosine triphosphate (ATP) (Guthrie *et al.* 1999), glutamate (Parpura *et al.* 1994), and D-serine (Schell *et al.* 1995). Astrocyte Ca^{2+} signalling, in particular, plays a significant crucial role in this bidirectional communication between astrocytes and neurons (Newman & Zahs, 1997; Grosche *et al.* 1999; Parri *et al.* 2001; Fellin *et al.* 2004; Fiacco & McCarthy, 2004; Newman, 2005; Perea & Araque, 2005*b*). Astrocyte Ca^{2+} activity coordinates synaptic networks and regulates synaptic strength and plasticity by Ca^{2+}-dependent ATP release (Pascual *et al.* 2005), which is hydrolysed into adenosine leading to persistent synaptic suppression.

In the retina, ATP and adenosine appear to be the principal neuromodulators involved in reciprocal neuron–glia signalling (Newman & Zahs, 1998; Newman, 2001, 2003, 2005; Metea & Newman, 2006; Stella *et al.* 2003). In addition, retinal ATP and adenosine levels exhibit circadian and light-dependent variations, with highest concentrations at night and in the dark, respectively (Stella *et al.* 2003; Ribelayga & Mangel, 2005). Neuron–glial communication may therefore be maximal in darkness and might be involved in dark-adaptive synaptic activity

This paper has online supplemental material.

DOI: 10.1113/jphysiol.2007.135715

(Wang & Mangel, 1996; Ribelayga *et al.* 2004) and plasticity (Behrens & Wagner, 1996). Until now, investigations of the dynamic changes of Ca^{2+} activity in the retina have been performed by using one- or two-photon laser-scanning microscopy with Ca^{2+}-sensitive fluorescent dyes, which can cause photoreceptor excitation (Denk & Detwiler, 1999). Glial Ca^{2+} activity measurements under complete darkness, when photoreceptors are not activated by light and when neuron–glial communication is expected to be highest, are highly desirable for understanding the involvement of this communication in dark-adaptive processes.

To address this question we developed a retinal glia-selective imaging method based on bioluminescent Ca^{2+} reporters. Here we used a genetically encoded bifunctional Ca^{2+} reporter called GFP (green fluorescent protein)-aequorin (GA) (Baubet *et al.* 2000), whose expression pattern can be monitored by GFP fluorescence (using light excitation) and Ca^{2+} activity measured by detection of bioluminescence. As opposed to fluorescent Ca^{2+} probes, the Ca^{2+}-induced bioluminescence produced by GA does not require light excitation, allowing imaging in darkness. After Ca^{2+} binding to aequorin, energy is transferred to GFP, whereby green light is emitted in a process known as chemiluminescence resonance energy transfer. By exposing retinal slices from adult mice to a viral vector expressing the cytoplasmic GA gene (Ad5-GA), we obtained a specific targeting of the main type of retinal glial cells, the Müller cells. Using bioluminescent Ca^{2+} imaging, we detected spontaneous Ca^{2+} changes in large populations of Müller cells in the retina under dark-adapted conditions. Combining statistical network analysis, we further established that retinal Müller cell spontaneous activity is organized in temporal networks of coactive cells. We showed that several of these networks are reactivated and could be sequentially reactivated, thereby revealing specific temporal dynamics.

Methods

Genetically encoded cytoplasmic GA Ca^{2+} reporter

We used the cytoplasmic GA whose energy transfer properties from aequorin to GFP have been previously described (Baubet *et al.* 2000). Briefly, the spectrum of GA emission mostly covers the spectrum of GFP emission, indicative of a good energy transfer between aequorin and GFP. The GA emission spectrum also slightly overlaps that of aequorin, indicating that some light may arise directly from aequorin.

Mouse retinal explant preparation and transfection with Ad5-GA

All animal care procedures and experimental protocols were in accordance with the recommendations of the European Community guidelines for laboratory animal handling. Retinal explants (neuronal retina co-cultured with retinal pigment epithelium) were obtained according to procedures previously described (Vallazza-Deschamps *et al.* 2005; Reidel *et al.* 2006). Six- to nine-week-old CBA mice (Janvier, France) were killed by cervical dislocation. After enucleation, eyes were incubated in Ames solution containing L-cysteine (0.035 mg) and papain (20 U, Worthington, Freehold, NJ, USA) for 45 min at 37°C. The enzymatic reaction was stopped by transferring the eyes to Dulbecco's modified Eagle's medium (DMEM) (Gibco, Life Technologies, Cergy-Pontoise, France) containing 10% fetal calf serum (FCS, Gibco) for 5 min at 4°C. A circular cut in the cornea was then made under the iris to remove the cornea, lens and vitreous. The remaining retina attached to the sclera was cut with four incisions from the retinal periphery toward the optic nerve head. The sclera was then peeled away leaving the retinal pigment epithelium (RPE) attached to the retina. The retina was finally flattened on a polycarbonate membrane in a culture dish (Costar Transwell, 3 μm pores, Corning Inc., USA) containing DMEM–10% FCS and 5×10^8 particles of Ad5-GA. The medium was adjusted to moisten the tissue by capillarity (~1.5 ml). Adult mouse retinal explants were conserved for 2 days *in vitro* in an incubator at 37°C and the culture medium was changed once after the first day. The explants were illuminated by the random opening of the incubator during daytime.

Combined fluorescence/bioluminescence imaging

Our fluorescence/bioluminescence wide-field microscopy system was custom made (ScienceWares Inc., MA, USA). Bioluminescence activity was detected using a highly sensitive image photon detector capable of detecting single photons and displaying high temporal resolution (IPD 3, Photek Ltd, East Sussex, UK) mounted on the baseport of a fully automated and inverted microscopy system (Zeiss, Germany). The system is housed in a light-tight dark box. The IPD detector system is a position-sensing high gain photomultiplier tube with a cascaded stack of four microchannel plates (MCP). Single photoelectron charge pulses generated by the MCP stack are collected by a two-dimensional resistive anode, which splits the charge pulses proportionally among four output corner electrodes. Electronic processing of the four simultaneous output charge pulses determines the *x*,*y* coordinates and time occurrence for each detected photon. The use of the IPD detector has been described in detail elsewhere (Webb *et al.* 1997; Gilland *et al.* 1999; Rogers *et al.* 2005). The IPD camera produces very low background counts (< 1 photon s^{-1} in a 256 pixel $\times$ 256 pixel region) and provides microsecond time resolution. The system is controlled by the data acquisition software, which

converts single photon event into an image that can be superimposed with brightfield or fluorescence images obtained with a CCD camera (Coolsnap HQ, Roper Scientific). Observations were made with ×25 or ×40 objectives.

After 2 days in culture, the polycarbonate membrane was cut out and placed on the base of a submersion-type recording chamber. Infected retinal explant, still fixed on the membrane, was held in place in the chamber with nylon threads attached to a platinum ring. The chamber was mounted on the inverted microscope and superfused (1–2.5 ml min^{-1}) with bicarbonate-buffered Ringer solution at room temperature. Superfusion of the preparation was halted after an initial 15 min period and GA was then reconstituted with wild type coelenterazine (Interchim, France). Because coelenterazine is an expensive reagent, 10 μM coelenterazine diluted in 250 μl of Hepes-buffered solution was added directly to the superfusion chamber and GA was reconstituted for 30 min. The slice was then equilibrated for at least 10 min by superfusing with Ringer solution. A fluorescence image focused on Müller cell bodies was taken and bioluminescence imaging started. After 1 h recording, the retinal explant was considered dark-adapted and the spontaneous Ca^{2+} activity over the next 2 h was subsequently recorded and kept for analysis. A second fluorescence image was taken at the end of the experiment in order to check the position of the sample. Currently the quantum efficiency of our IPD detector is low (< 10%) compared to the newly developed CCD camera. However, the signal-to-noise ratio is excellent because photons are detected over an almost dark background since the detector itself displays a very low dark noise. Thus, even if the signals detected consist of a few photons, they are indicative of local Ca^{2+} changes. In addition, the dynamic range of GA is 0.1–10 μM, which is at the upper range of cytosolic Ca^{2+} concentration under resting conditions (50–100 nM, Rizzuto & Pozzan, 2006), allowing the detection of active cells only.

Note that Müller cells were often found in radial position on the edge of the explants where the tissue border was folded and it was thus possible to visualize Ca^{2+} increases in microdomains within both processes and soma of Müller cells (Fig. 3). Otherwise, in the majority of cases (Figs 2, 4, 5 and 7), Ca^{2+} activity occurring within the inner processes of a large number of Müller cells was visualized across the inner vitreal surface of the flat-mounted retina.

Superfusion preparations

The Hepes-buffered solution contained: NaCl (129 mM), KCl (5 mM), $CaCl_2$ (2 mM), $MgCl_2$ (2 mM), D-glucose (30 mM), Hepes (25 mM) and glycine (10 μM). The Ringer solution contained: NaCl (117 mM), KCl (3 mM), $CaCl_2$ (2 mM), $MgSO_4$ (1 mM), NaH_2PO_4 (0.5 mM), D-glucose (15 mM), $NaHCO_3$ (32 mM) and L-glutamate (0.01 mM); the solution was equilibrated with 5% CO_2 in O_2.

Immunohistochemistry

Slices were fixed for 10 min in 4% paraformaldehyde diluted in 1X PBS, pH 7.4, frozen and cut into 12 μm sections. Tissue sections were treated for 30 min in 1X PBS containing 0.2% gelatin and 0.25% Triton X-100 pH 7.4, and incubated overnight in this buffer with one of the following antibodies: (1) Müller cell marker mouse anti-S-100 β (S-100 β, 1 : 1000, Sigma); (2) astrocyte marker goat anti-glial fibrillary protein (GFAP, 1 : 1000, Santa Cruz Biotechnology, Inc.); (3) neuronal bipolar cell marker mouse anti-protein kinase C α (PKC α, 1/100, Santa Cruz Biotechnology, Inc.); (4) neuronal photoreceptor marker mouse anti-Opsin (1/5000, Sigma); (5) neuronal ganglion cell marker goat anti-Brn-3 (Brn-3, 1/2500, Santa Cruz Biotechnology, Inc.); (6) neuronal marker mouse anti-neuronal nuclei (NeuN, 1 : 2500, Chemicon International); (7) neuronal horizontal/amacrine cell mouse anti-calbindin-D-28K (1 : 1000, Sigma). The sections were then rinsed 4 times in the same buffer for 15 min each, incubated 90 min with corresponding secondary antibodies: Cy3-conjugated anti-mouse antibody (1 : 1000, Sigma) or Alexa 546-conjugated anti-goat (1 : 1000, Molecular Probes). Sections were subsequently washed in 1X PBS for 30 min and mounted with Fluoromont G solution. All steps were performed at room temperature.

Activity, network and statistical analysis

Regions of interest (ROIs = 10 μm × 10 μm squares approx. the size of the Müller cell body or end-foot) were automatically detected from bioluminescence images (each image corresponds to 4 s of accumulated light) with a Visual Basic program described elsewhere (Platel *et al.* 2005, 2007). ROIs were then superimposed over the corresponding fluorescence image focused preferentially on Müller cell bodies in order to check that bioluminescent signals were generated by actual cells. The threshold used to detect activity was 1 photon ROI^{-1} $(4\ s)^{-1}$, so signals ≥ 2 photons ROI^{-1} $(4\ s)^{-1}$ were scored as Ca^{2+} signals within individual cells. After detection of Ca^{2+} transients, their main parameters (amplitude, duration and frequency) were calculated and summarized in Microsoft Excel sheets from which global analysis was performed (data compiling, statistical tests, etc.).

Based on raster plots of bioluminescence peaks, χ^2 contingency tables were used to calculate significant coactivations of cells within slices ($P < 0.05$). Monte Carlo simulations were then performed to show that the detected spontaneous activities were significantly more

synchronous than expected by chance: 1000 simulations of each retinal slice, using the same number of active ROIs, peaks and time were performed and the number of simulations displaying more coactivations than the real data constituted the statistical test p_{MC}. Significant network synchrony was established when $p_{MC} < 0.05$, thus defining networks of synchronously active Müller glial cells.

Numerical values are given as mean ± S.E.M.

Retinal ganglion cell electrophysiological recording

Dark-adapted (1 h) retinal explants fixed on the polycarbonate membrane were placed with the neuronal ganglion cell layer face down into a 3-D microelectrode array (MEA60) recording chamber (Ayanda Biosystems S.A., Switzerland) under dim red light. The tissue was continuously superfused at room temperature or at 37°C. Recordings were obtained from both central and peripheral retina. For electrophysiological recordings we used MEA60 arrays of 60 3-D tip-shaped platinum electrodes (electrode height: 50-70 μm, electrode spacing 200 μm, centre to centre). A commercial 60-channel amplifier (MEA1060, Multi Channel Systems MCS GmbH, Germany) was used to acquire extracellular action potentials. Extracellular activity was filtered on-line, band-passed and sampled at 25 kHz using a 52000a/56 analog-to-digital board, and analysed with MC_Rack data acquisition software (MEA60 setup, Multi Channel Systems) and Spike2 software (Cambridge Electronic Design Ltd, UK).

Results

Specific expression of the cytoplasmic Ca^{2+} reporter GFP-aequorin in the Müller glial cells of adult retinal explants

Two-day exposure of organotypic retinal slices from adult mice to an adenovirus expressing the cytoplasmic Ca^{2+} reporter GA resulted in green staining of a subpopulation of retinal cells. Using confocal microscopy, the viral vector was found to be selectively taken up by 70% of Müller cells (Fig. 1*A*–*C*), which are the predominant class of glial cells in the vertebrate retina (Newman & Reichenbach, 1996). Transfected cells were widely and equally distributed all over the retinal explants and did not present any specific pattern of distribution. No expression of GA was detectable in astrocytes, which are the second glial cell type of the retina (Fig. 1*D*). By using antibodies directed against markers of the different neuronal cells of the retina, we did not find any detectable expression of GA in neurons (Fig. 1*E* and data not shown). The mechanism for selective uptake of the GA-expressing adenovirus by Müller cells is unknown, but could be explained by cell morphology and distribution. Müller cells span the entire width of the retina from the outer limitant membrane to the inner side, where they terminate in expanded end-feet, forming a border adjacent to the vitreous humour (Newman & Reichenbach, 1996; Fig. 1*A*). This makes Müller cells directly accessible at the inner vitreal surface, in contrast to retinal neurons, so that the viral vector may more effectively enter Müller cells, resulting in a specific viral infection and cytoplasmic GA expression.

Spontaneous Ca^{2+} transients in Müller cells

To analyse the spontaneous Müller cell Ca^{2+} signalling characteristics under dark conditions, we imaged retinal explants previously infected with Ad5-GA over 1 to 2 h in constant darkness. Recordings were conducted by monitoring photon emission across the inner surface of flat-mounted retina explants (Fig. 2*A*). Indeed, by virtue of the transretinal, radial and well-organized Müller cell orientation, we found that recording Ca^{2+} signals across the retinal inner surface allowed ready detection of bioluminescent photons in local areas, which overlapped individual Müller cell bodies, processes (Fig. 2*A*), or end-feet on fluorescence images. We imaged long-lasting spontaneous activity (Fig. 2*B*). Since bioluminescent photons can penetrate small tissue depth without being absorbed significantly, they are likely to be emitted from inner processes and/or end-feet of individual Müller cells when detected. To check whether there were spontaneous Ca^{2+} transients occurring in inner parts of Müller cells, we imaged radially orientated Müller cells in several slices (Fig. 3). We found that Ca^{2+} increases were mostly generated in processes within the inner plexiform layer, the ganglion cell layer and cell end-feet of individual Müller cells, but rarely observed in the outer parts of processes and soma (Fig. 3*A* and *B*, and data not shown). These results showed that Ca^{2+} events imaged across the inner surface of flat-mounted retinas (Figs 2, 4, 5 and 7) are from inner processes of individual Müller cells. These Ca^{2+} signals observed were confined to a microdomain (Fig. 3*C* and corresponding Movie 1 in online Supplemental material) or propagated as an intracellular Ca^{2+} wave along the Müller cell inner process (Fig. 3*D* and corresponding Supplemental Movie 2).

We then quantified the characteristics of the observed Ca^{2+} changes in order to determine spatiotemporal organization displayed by groups of Müller cells in flat-mounted retinal explants. We previously reported that the dynamic range for measuring cytosolic Ca^{2+} concentrations when using GA is 0.1–10 μM (Rogers *et al.* 2005), indicating that each photon emitted corresponds to micromolar variations of Ca^{2+} concentration, which is much higher than cytosolic concentration under resting conditions (50–100 nM). In addition, our photon detector produces very low background counts (< 1 photon s^{-1}

in a 256 pixel × 256 pixel region, i.e. the entire retinal field). Finally, we observed that spontaneous Ca^{2+} transients were long (Figs 2*B*, and 3*C* and *D*). Therefore, we chose to analyse signals higher than 1 photon in 4 s time frames of accumulated light within regions of interest (ROIs = 10 μm × 10 μm square, approx. the size of the Müller cell body and end-foot) across the inner retinal surface. Regions of interest were automatically drawn over active regions detected in the entire retinal field using software described elsewhere (Platel *et al.* 2005, 2007). Then, superimposition of ROIs on the corresponding fluorescence image enabled unambiguous identification of Müller cell bodies (Fig. 4*A*–*C*). Most ROIs overlapped Müller cell bodies, indicating that luminescence signals were indeed generated by individual Müller cells. A few ROIs that did not overlap cell bodies were manually removed from the analysis. Over 10 retinal slices, representing 506 detected active individual cells and 1820 Ca^{2+} events, we found that Ca^{2+} transients displayed a mean duration of 7.49 ± 0.84 s (up to 36 s), a mean peak amplitude of 3.11 ± 0.22 photons (up to 15 photons), and a mean total number of photons per Ca^{2+} event of

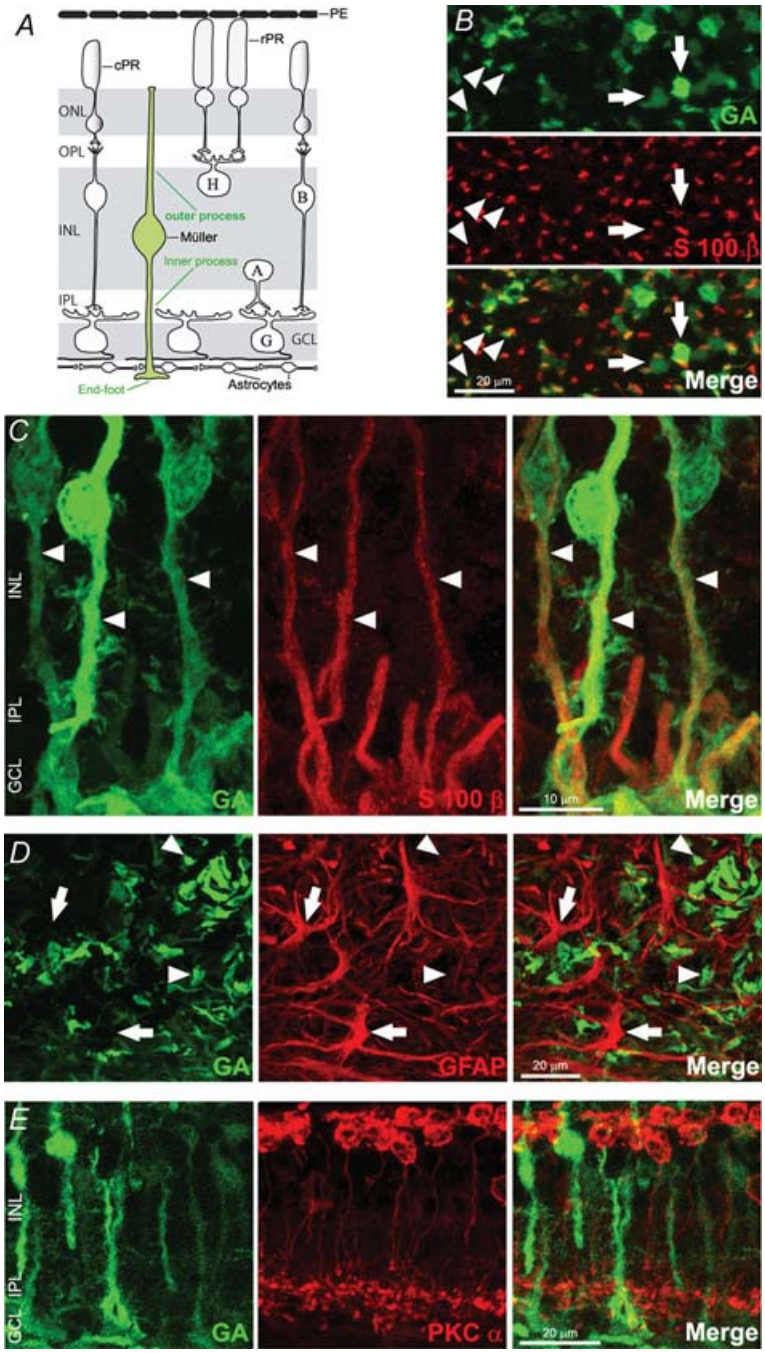

Figure 1. Specific expression of the cytoplasmic Ca^{2+} reporter GA in Müller glial cells of retinal organotypic explants
A, schematic diagram of the retina showing the localization of the different cell types. *B* and *C*, GA (green) was specifically expressed in astrocytic Müller cells readily identifiable by their unique morphology and by subsequent immunochemical labelling with an antibody against the specific marker of Müller cells, S-100 β-subunit (red). *B*, sections through the inner nuclear layer (INL) of flat-mounted retina show soma (arrows) and processes of Müller cells (arrowheads), which were visible as fluorescence-marked structures (GA in green, S-100 β-subunit in red). Note that because S-100 β-subunit localization is adjacent to the cell membrane whereas GA localization is cytoplasmic, the co-localization is partial. *C*, radial sections through the INL, the inner plexiform layer (IPL) and the ganglion cell layer (GCL) show that GA is expressed in soma and inner processes of Müller cells (arrowheads). *D*, in the GCL–vitreal inner surface of flat-mounted retina, GA (green, arrowheads) expression was not found in glial fibrillary protein (GFAP)-expressing astrocytes (red and arrows), indicating that the green structures corresponded to the inner processes/end-feet of Müller cells. *E*, GA (green) was not detected in protein kinase Cα-expressing neuronal bipolar cells (red). Abbreviations, A, amacrine cell; B, bipolar cell; cPR, cone photoreceptor; G, ganglion cell; GCL, ganglion cell layer; H, horizontal cell; INL, inner nuclear layer; IPL, inner plexiform layer; ONL, outer nuclear layer; OPL, outer plexiform layer; PE, pigment epithelium; rPR, rod photoreceptor.

20.7 ± 5.58 photons (up to 64 photons). The mean rate of Ca^{2+} transients was 1.31 ± 0.29 Ca^{2+} events (active cell)$^{-1}$ (1000 s)$^{-1}$ (up to 4.72 events (active cell)$^{-1}$ (1000 s)$^{-1}$).

Spontaneous Müller glial cell activity is organized into correlated networks

Because previous data performed on P5–P7 postnatal and juvenile brain revealed that astrocytes showed correlated spontaneous Ca^{2+} increases, indicative of coordinated activity (Aguado *et al.* 2002; Hirase *et al.* 2004), we inquired whether the same was true for Müller astrocyte cells of adult retina. Active Müller cells were detected (Fig. 4*A–C*) as described above and statistical correlations were calculated (see Methods). Spontaneous Ca^{2+} activity observed in 12 retinal slices representing 614 Müller cells (47.23 ± 4.30 active cells (slice)$^{-1}$) was transformed over time into raster plots in which the time of initiation of each Ca^{2+} transient was marked (Fig. 4*D*). Using contingency χ^2 tables, significant coactivations between pairs of cells (see Methods) were identified and represented on correlation maps (Fig. 4*E*), as described elsewhere (Platel *et al.* 2007). To quantify the degree of network synchrony present in the data set, 1000 Monte Carlo simulations of each raster plot were performed and the number of simulated significant coactivations was calculated (Fig. 4*F*). In the example considered, no simulation displayed as many coactivations as the experimental data set, indicating highly significant network synchrony in the retinal slice among Müller cells ($p_{MC} < 0.001$, Fig. 4*F*). In a larger set of data, we found that spontaneous Ca^{2+} transients were organized into complex synchronous networks that recruited 2–16 coactivated neighbouring and/or distant Müller cells (9.08 ± 1.11 coactivated cells per slice, $n = 12$ slices). Quantitative analysis of network synchrony showed 68.1 ± 4.7% of active Müller cells participated in correlated networks and that the average distance between coactive pairs of Müller cells was 51.72 ± 3.93 μm, whereas the distance between uncorrelated pairs was 122.87 ± 2.28 μm ($P < 0.05$).

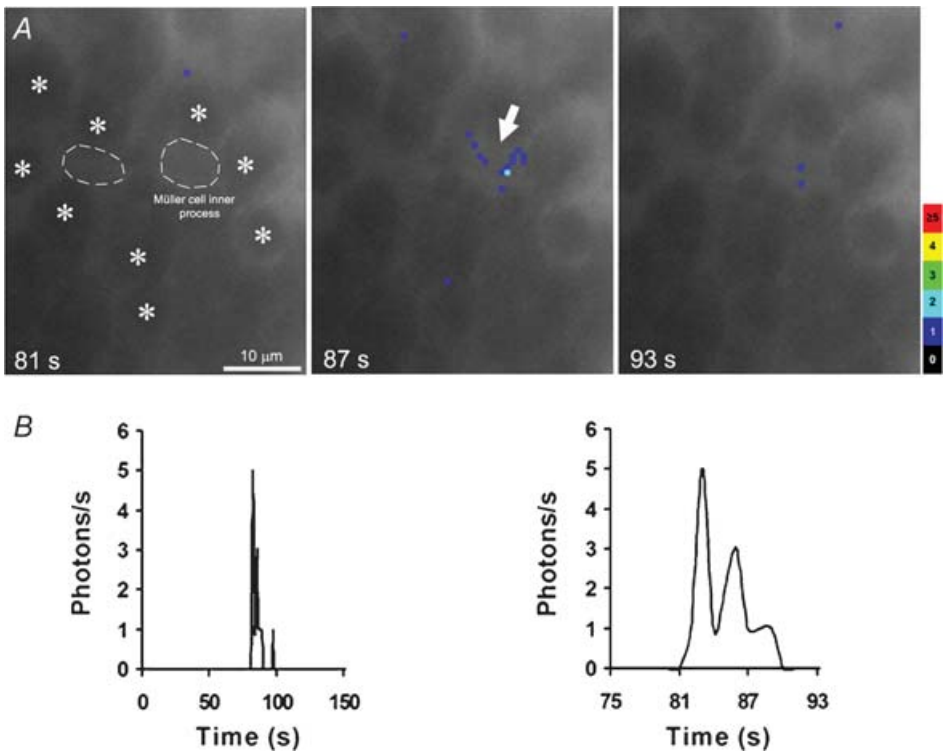

Figure 2. Bioluminescence imaging across the inner surface of flat-mounted retinal allows the measurement of spontaneous Ca^{2+} events occurring within inner processes and end-feet of individual Müller cells

A, superimposition of bioluminescence images obtained from photons emitted across the inner surface of flat-mounted retinal explants over corresponding fluorescence image focused on the GCL: bioluminescent photons are detected in local areas (blue pixels, arrow) overlapping individual Müller cell processes (dotted line and arrow). Luminescence images correspond to 6 s of accumulated light and light emission is coded (photons pixel^{-1}) in pseudocolours. Stars mark ganglion cell bodies. *B*, bioluminescence (photons s^{-1}) detected within an individual Müller cell process (arrow in *A*) plotted over 150 s (left panel) or shown with an expanded time scale (right panel) revealing a Ca^{2+} event that lasted 9 s.

Neuronal activity regulates the correlated network properties of spontaneous Müller cell activity

Given that neuron-to-Müller cell signalling is mediated by neurotransmitter release from ganglion and/or amacrine cells under light conditions (Newman, 2005), we tested the hypothesis that Ca^{2+} transients observed under dark conditions were caused or regulated by action potentials in these neuronal cell types. We measured activity following the application of TTX (1 μM, 1 h) to abolish action potentials in ganglion and amacrine cells, the two kinds of retinal neurons generating action potentials, and found a small but significant decrease in the number of active Müller cells exhibiting spontaneous Ca^{2+} activity (decrease to 69.4 $\pm$ 11.4% of control, $P = 0.02$, $n = 6$ slices, Fig. 5*C*). However, the rate of Ca^{2+} transients in the remaining active Müller cells was unchanged (Fig. 5*C*), indicating that ganglion and/or amacrine cell activity was not required for the generation of their spontaneous Ca^{2+} activity. Interestingly, the TTX-induced Na^{+} channel blockade dramatically impaired network synchrony in the remaining active cells, resulting in very simple networks (Fig. 5*B*, *B*1 and *C*). We found that the number of coactive pairs/slice was 129.47 $\pm$ 42.47 in basal conditions *versus* 25.50 $\pm$ 7.23 in TTX conditions ($P = 0.02$, $n = 6$ slices). Taken together, the minor effect on the number of active Müller cells, the absence of a significant effect in the activation rate and the loss of correlated networks indicate

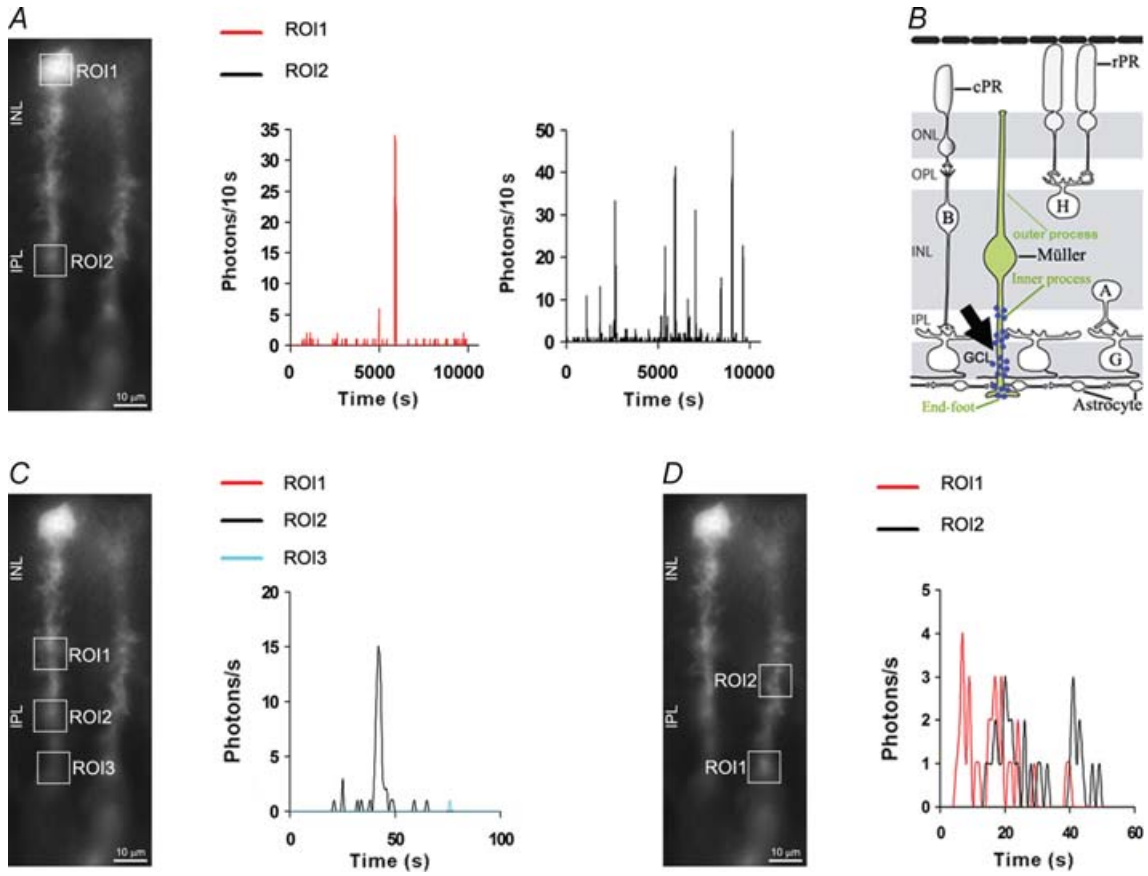

Figure 3. Spontaneous Ca^{2+} transients are mostly generated within microdomains of Müller cell inner processes

A, fluorescence image of radially orientated Müller cells with two selected regions of interest (ROI1 and ROI2) and bioluminescence (photons (10 s)$^{-1}$) from ROI1 and ROI2 plotted over more than 2 h. Graphs show that Ca^{2+} events were mostly observed in the inner parts of Müller cells (ROI2) as compared to the soma (ROI1). *B*, schematic diagram of the retina showing that spontaneous Ca^{2+} increases are most frequently detected in inner Müller cell processes within the IPL, the GCL and end-feet. Blue dots (arrow) represent the photons emitted within the inner processes of Müller cells. *C*, bioluminescence (photons s^{-1}) from three microdomains (ROI1–ROI3) within the same inner Müller cell process, plotted over 100 s on the same graph. Note that Ca^{2+} activity was not found in ROI1 and ROI3 indicating that activity detected in ROI2 did not propagate. *D*, bioluminescence (photons s^{-1}) from two microdomains (ROI1, ROI2) within the same inner Müller cell process, plotted over 60 s on the same graph. Traces indicate that the Ca^{2+} increase started in ROI1 and then spread into the process up to ROI2 as an intracellular Ca^{2+} wave. Abbreviations, A, amacrine cell; B, bipolar cell; cPR, cone photoreceptor; G, ganglion cell; GCL, ganglion cell layer; H, horizontal cell; INL, inner nuclear layer; IPL, inner plexiform layer; ONL, outer nuclear layer; OPL, outer plexiform layer; PE, pigment epithelium; rPR, rod photoreceptor.

that spontaneous Ca^{2+} transients still occur but become uncorrelated after TTX treatment. These data demonstrate that ganglion and/or amacrine cells control Müller cell network properties.

In order to confirm the presence of spontaneously discharging ganglion cells in our dark-adapted retinal explants, single-unit activity was recorded extracellularly using a multi electrode array technique. Ganglion cells were found to spontaneously discharge, and the typical characteristics of their activity are illustrated in Fig. 6*A* and *B* ($n = 6$ slices). Stable recordings from several electrodes (up to 11) could be simultaneously monitored with a

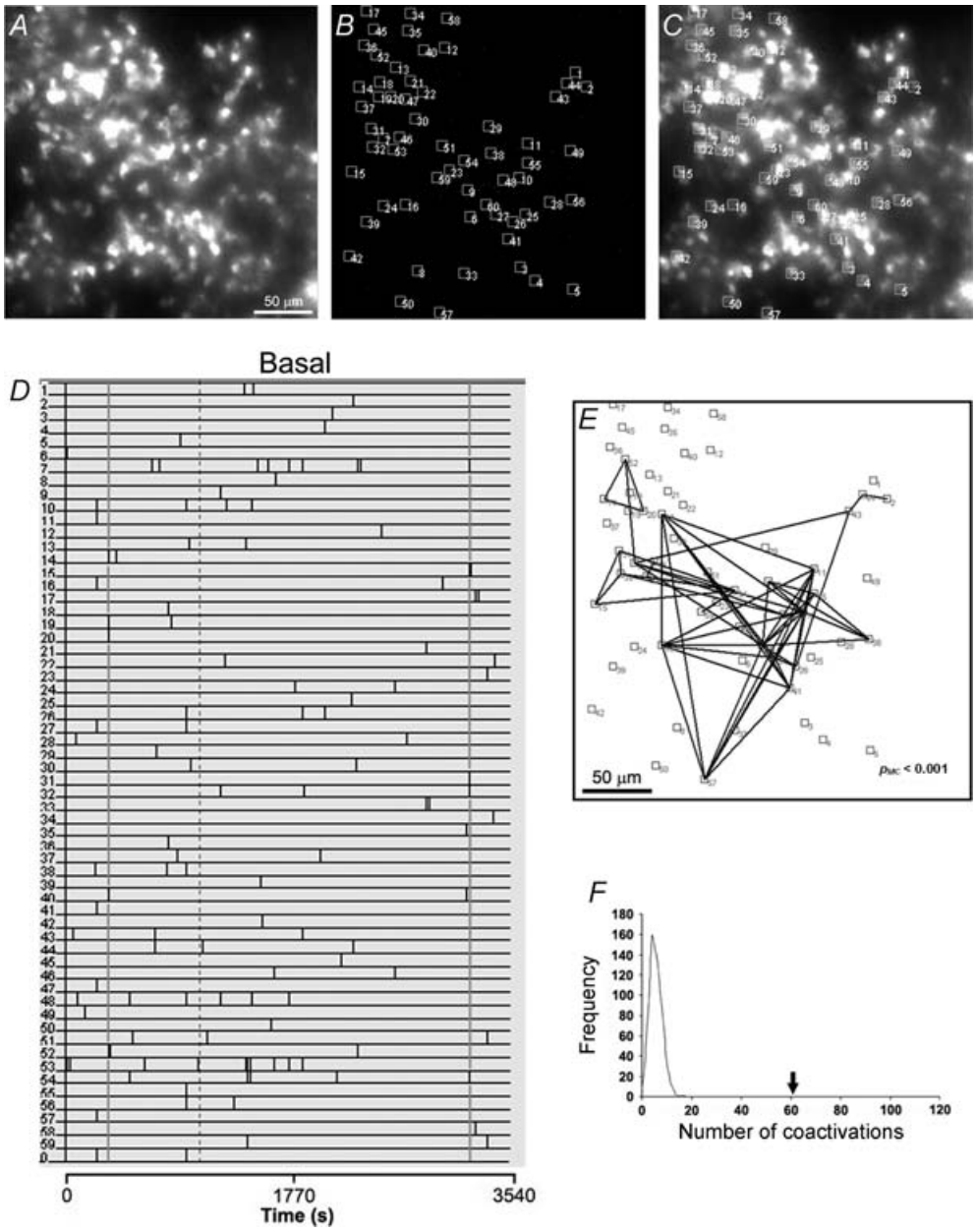

Figure 4. Spontaneous Ca^{2+} transients in Müller glial cells are organized in correlated networks
A, fluorescence image of a large retinal explant area focused on Müller cell bodies, taken at the beginning of the experiment (representative example). *B*, automatically detected ROIs (10 μm × 10 μm squares) corresponding to active areas over almost 1 h. *C*, superimposition of detected active ROIs over the corresponding fluorescence image. *D*, corresponding raster plot of Ca^{2+} transients detected within active Müller cells. Vertical lines show synchronous activity in different cells. *E*, correlation map showing significant coactivations between pairs of active cells detected in *B*, calculated with χ^2 tables (see Methods). Cells with statistically significant correlation coefficients are connected by lines. *F*, number of significant coactivations detected in the representative example presented above (arrow) *versus* 1000 Monte Carlo simulations of the raster plot displayed in *D* (curve) and significancy index $p_{MC} < 0.001$.

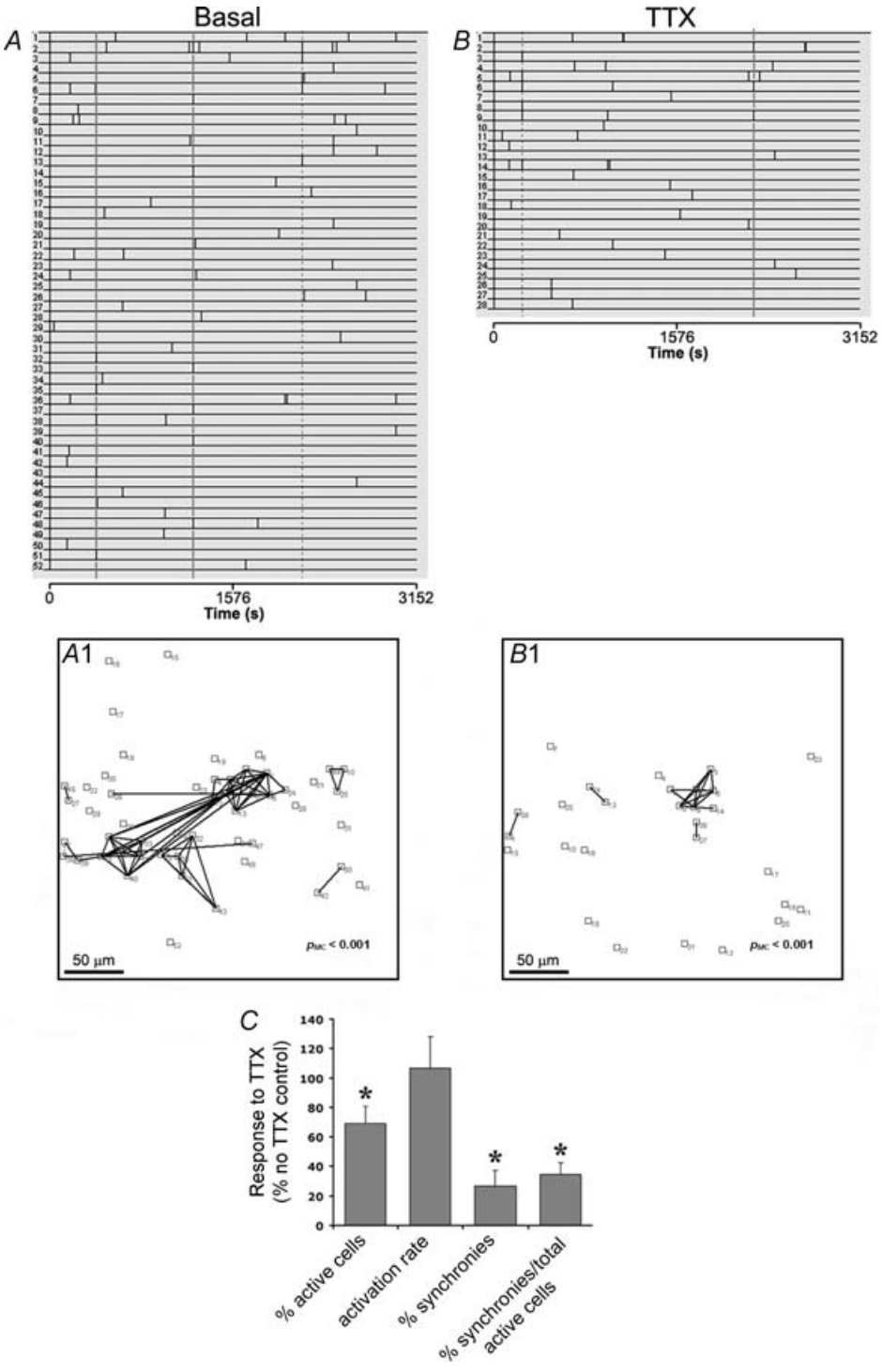

Figure 5. Synchronous networks of spontaneous Ca^{2+} transients are regulated by neuronal activity
A, raster plot of spontaneous Ca^{2+} activity of a representative retinal sample recorded over 53 min in basal conditions. Vertical lines show synchronous activity in different cells. *A*1, correlation map corresponding to *A* and showing active cells (10 μm × 10 μm squares) and significant coactivations (lines, see Methods). *B*, raster plot of spontaneous Ca^{2+} activity after TTX (1 μM, 53 min) administration on the same retinal sample. Vertical lines show synchronous activity in different cells. *B*1, correlation map corresponding to *B* and showing active cells (10 μm × 10 μm squares) and significant coactivations (lines, see Methods). *C*, histogram (% control, mean ± S.E.M., $n = 6$ slices) illustrating the effect of TTX on the percentage of active Müller cells per slice, activation rate of active cells, percentage of synchronies (i.e. coactive pairs) per slice and percentage of synchronies per total active cells detected per slice. Statistical significance was determined with Student's two-tailed *t* and/or Wilcoxon tests ($P < 0.05$).

good signal/noise ratio over 3 h. The spontaneous activity ranged from 0.2 to 5 Hz, and occasionally reached 15 Hz. These results demonstrate the presence of spontaneously active ganglion cells displaying typical patterns of activity.

Spontaneous activity of correlated networks of Müller glia can repeat, and some repetitions occur in a precise sequential order

Since neuronal activity regulates Müller cell network properties (Fig. 5), and because repeated synchronous activity of neurons organized in networks has been observed in retina and brain (Lagnado & Baylor, 1995; Neuenschwander & Singer, 1996; Neuenschwander *et al.* 1999; Ikegaya *et al.* 2004), we aimed at identifying recurring activity of the same synchronous Müller cell networks. Multiple correlations of two or more Müller cells are very unlikely to emerge by chance, given the multiplicative effect of low probabilities for single occurrence of correlated pairs (as shown by the *P* value obtained from Monte Carlo simulations). We systematically searched raster plots and correlation maps for such repetitions of synchronous networks and found that they were not uncommon, being present in 6 of 12 slices ($n = 218$ repeating networks, mean $= 18.17 \pm 4.19$ repeating networks per slice, ranging from 0 to 48, $n = 12$ slices). They involved 2–6 cells and repeated 2–5 times h^{-1} (Fig. 7*A*–*C*, and data not shown). Correlations between pairs (Fig. 7*A*) could repeat up to 5 times h^{-1}, while correlations in 3 to 6 cell groups of (Fig. 7*B*) only repeated 2 or 3 times per hour. Moreover, when examining the temporal pattern of such repeating networks, we observed that series of networks were activated in the same sequential order twice per hour ($n = 6$ slices, Fig. 7*C*) and some networks participated in several different sequences.

We further characterized the spatial structure of these repeated networks and found that networks had different topographic structures (Fig. 7*C*, correlation maps), involving pairs or groups of cells located distantly and/or in clusters. In many cases, individual Müller cells participated simultaneously or sequentially in more than one network (Fig. 7*B*, cells 1 and 7; Fig. 7*C*, cell 21, left panel, and Fig. 7*C*, cells 7 and 19, right panel) and different networks of correlated Müller cells could overlap in the same spatial regions (Fig. 7*C*, correlation map, right panel). Moreover, bath application of TTX, which led to a dramatic decrease in the total number of synchronous networks (Fig. 5*B*, *B*1 and *C*), decreased the number of repeating networks to $9.0 \pm 4.8\%$ of control ($n = 6$ slices), indicating that ganglion and/or amacrine cells regulate both correlated networks and repeating correlated networks.

Figure 6. Spontaneous activity of retinal ganglion cells recorded extracellularly from retinal organotypic explants ($n = 6$) using the MEA60 system
A, single trace showing spontaneous multi-unit activity recorded from 1 of 60 electrodes. *B*, expanded spike from trace in *A* showing a typical ganglion cell action potential.

Discussion

In this study, we investigated the characteristics of spontaneous Ca^{2+} dynamic changes in Müller cells under dark conditions by using a bioluminescence imaging method in retinal glia. We show that Müller cells *in situ* display long-lasting spontaneous activity. Moreover, our observations indicate, for the first time, that activity of glial cells in adult retina is patterned into synchronous networks, which can repeatedly activate over time, in the same sequential order, and are regulated by neuronal activity. This result significantly extends the known properties of glial cells in adult retina and also raises the possibility that these spontaneous correlated networks and their repetitions occur in other regions of the adult central nervous system (CNS).

By comparison with other techniques that are currently available for monitoring glial Ca^{2+} activity in retina, the bioluminescence imaging method used in this study offers three major improvements. First, optical Müller cell Ca^{2+} imaging can be carried out in the absence of external illumination. Indeed, although infrared illumination used for two-photon imaging does not overlap spectral sensitivity of most visual pigments (Denk & Detwiler, 1999), some photoreceptors display photopigment spectral sensitivity shifted toward infrared wavelengths (Makino & Dodd, 1996). However, we cannot exclude the possibility that some bioluminescent photons emitted from GFP-aequorin within the inner processes and end-feet of Müller cells could cross the inner nuclear layer (INL) and the outer plexiform layer (OPL), reach the outer nuclear layer (ONL), and then change the level of activity of rod photoreceptors and contribute to the pattern of Müller cell activity. However, this must be a rare phenomenon since emitted photons can go in any direction and not only in the direction of the retinal outer surface where photoreceptors are located. More importantly, it is very unlikely that photons emitted from a single Müller cell repetitively activate the same rod

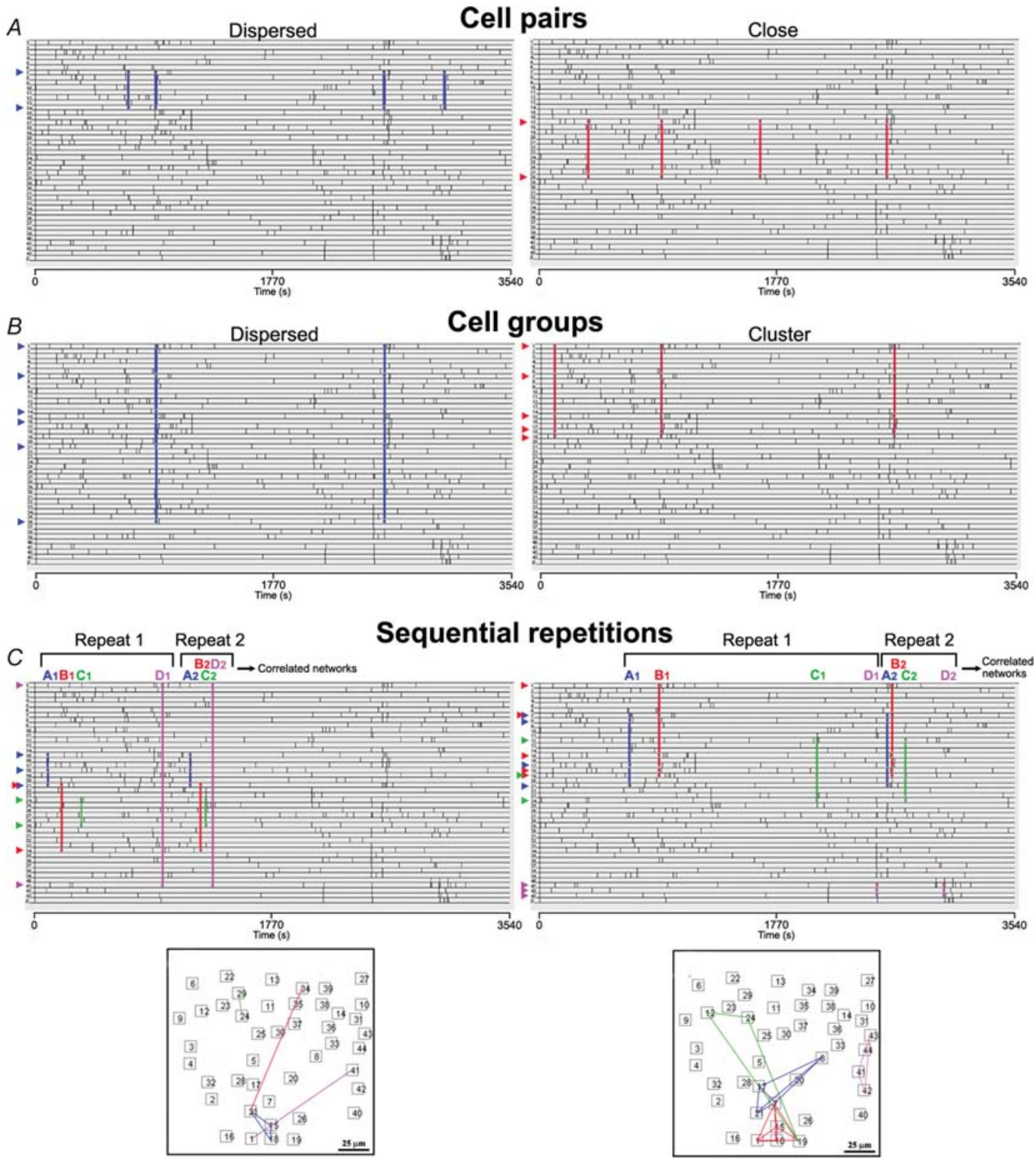

Figure 7. Reactivations of synchronous networks (*A* and *B*) and sequential reactivations of series of networks (*C*) found in the same representative sample

A, raster plots with pairs of Müller cells coactivated 4 times over 1 h. The left panel shows 2 distant cells (blue, distance = 91.45 μm) while the right panel shows 2 neighbouring cells (red, distance = 12.5 μm). *B*, raster plots with networks involving more than 2 coactive Müller cells, which reactivated twice (blue, left panel) or 3 times (red, right panel) over 1 h. The left panel shows a correlated network involving 4 neighbouring and 2 distant cells (blue, average distance = 73.47 μm), while the right panel shows a cluster of 5 neighbouring cells (red, average distance = 26.97 μm). *C*, representative raster plots with series of synchronous networks repeating twice in the same sequential order over 1 h (left and right panels) and corresponding correlation maps where each network of coactive cells is represented. Networks consisted of 2–5 neighbouring and/or distant Müller cells.

photoreceptor. Such a rare and random phenomenon probably does not contribute to the statistically significant repetitive and coordinated Ca^{2+} transients, synchronized over space and time in Müller cells. The second improvement is that this bioluminescence approach is specific for a unique glial cell type, the Müller glial cell, which plays an important role in neuron–glia communication (Newman & Zahs, 1998; Newman, 2003, 2005) and represents a model for studying the role of glia in dark-adaptive retinal synaptic activity and plasticity processes. The last major improvement is that phototoxicity is greatly reduced since the sample is not illuminated. Thus, such non-phototoxic imaging can be done over long periods, allowing the recording of a larger number of infrequent Müller cell Ca^{2+} events than would be possible using fluorescence-based methods. It also provides the opportunity to analyse spatiotemporal dynamic changes of retinal networks over hours, thereby enabling detection of temporal patterns of correlated network activity.

Finally, the absence of background in bioluminescence microscopy results in an excellent signal-to-noise ratio. Even though the spatial resolution of luminescence microscopy is significantly lower than confocal-type resolution, our method enables real-time and large-scale monitoring of simultaneous Ca^{2+} increases with single-cell resolution as compared to other microscopy methods (Newman, 2005; Ikegaya *et al.* 2005).

To date, one study has reported spontaneous Ca^{2+} transients in Müller cells of adult retina (Newman, 2005). As in our study, Ca^{2+} oscillations were observed to occur primarily within the inner plexiform layer, which is the principal synaptic layer of the retina. Although this previous study (Newman, 2005) used acute slices of rat retina under constant illumination, while we worked on organotypic slices of mouse retina under dark conditions, the similarity in the obtained results suggests that Müller cell activation is a common feature of neuron–Müller cell crosstalk in retina under light as well as dark conditions. However, since more than 80% of the cytoplasmic volume of Müller cells is located in the end-feet and inner processes, we cannot rule out the possibility that Ca^{2+} increases occurred in the outer processes, but were difficult to detect.

We and Newman (2005) found that spontaneous Ca^{2+} transient durations in Müller cells of adult retina are 2- to 4-fold shorter than durations previously described in astrocytes of postnatal and juvenile brain (Parri *et al.* 2001; Aguado *et al.* 2002; Hirase *et al.* 2004), suggesting the existence of activity differences between retinal Müller glial cells and brain astrocytes and/or maturity differences (adult *versus* postnatal/juvenile).

We have shown that activity emerging from groups of neighbouring and/or distant Müller cells is patterned into synchronous networks. Although most active Müller cells are not driven by ganglion or amacrine cells (Fig. 5*C*), these neuronal cell types control Müller cell network activation, probably by action potential-dependent release of neurotransmitters. A similar dependence of astrocyte network activation on neuronal activity has been demonstrated in P5–P7 postnatal brain (Aguado *et al.* 2002). To our knowledge, our results demonstrate for the first time that spontaneous glial activity may be organized in synchronous networks in adult CNS and regulated by neuronal activity. Müller cell-coordinated activity might depend on the integration and processing (Perea & Araque, 2005*b*) of spatially distributed and simultaneous synaptic network information. This view is supported by our data showing spontaneous discharges in ganglion cells (Fig. 6), and previous data showing the occurrence of spontaneous and light-evoked synchronized discharges in segregated ensembles of ganglion cells (Lagnado & Baylor, 1995; Meister *et al.* 1995; Neuenschwander & Singer, 1996). Such neuronal synchronization might favour correlation of spatially dispersed Müller cells. Furthermore, the different temporal properties of neuronal and Müller activity (several orders difference in frequencies), might suggest that the correlated activity in networks of Müller cells was not dependent on the frequency of activity of individual ganglion cells, but rather on a specific (less frequent) combination of coactive ganglion cells.

An unexpected finding of the present study was the existence of repeated dynamics in the glial network activity over 30–40 min. These networks can be modules of larger temporal structures, defined by their sequential order of activation. The mechanism that generates repetitions of Müller cell network activity appears to be independent of light stimulation and intrinsic to the retinal circuit because repetitions are preserved in dark-adapted slices. It may be linked to recurrent activity of specific networks of synchronized neuronal cells. Data reporting oscillatory activity in ganglion cells that synchronize (Lagnado & Baylor, 1995; Neuenschwander *et al.* 1999; Fig. 6), as well as the fact that ganglion and/or amacrine cells regulate these repetitions (Fig. 5), suggest that these neuron types are involved in repeated Müller cell activation. Thus, regardless of the underlying mechanisms and their importance in dark-adaptive processes, our study provides the first evidence that neuron-to-glia signalling in retina may control rhythmic patterns in glial network activity.

Conclusions

The repetitive activity of Müller cell networks detected in our study indicate that the retinal microcircuit cannot only sustain spontaneous activity under dark conditions, but is capable of generating repeated patterns of coordinated activation. These particular network properties might reflect oscillatory coordinated activity of the underlying neuronal circuits, either ongoing or secondary to

dark-adaptive circuit activation processes. Furthermore, because reciprocal Müller cell-to-neuron communication has also been demonstrated previously (Newman & Zahs, 1998; Newman, 2003, 2005), Müller cells might influence the overall dynamics of neuronal activity, acting to modulate (favouring or depressing) the formation of dynamically associated assemblies of neurons.

Finally, since GA is a genetically encoded Ca^{2+} reporter, this probe can be targeted to defined subpopulations of retinal and CNS cells of transgenic animals. Therefore, the bioluminescence imaging approach combined to network analysis methodology will provide in the future a unique tool to visualize Ca^{2+} activity and reconstruct the network dynamic characteristics of specific glial and neuronal cells in various tissues, and investigate their reciprocal communication on acute retinal slices over long periods of time.

References

Aguado F, Espinosa-Parrilla JF, Carmona MA & Soriano E (2002). Neuronal activity regulates correlated network properties of spontaneous calcium transients in astrocytes in situ. *J Neurosci* **22**, 9430–9444.

Baubet V, Le Mouellic H, Campbell AK, Lucas-Meunier E, Fossier P & Brulet P (2000). Chimeric green fluorescent protein-aequorin as bioluminescent Ca^{2+} reporters at the single-cell level. *Proc Natl Acad Sci U S A* **97**, 7260–7265.

Behrens UD & Wagner HJ (1996). Adaptation-dependent changes of bipolar cell terminals in fish retina: effects on overall morphology and spinule formation in Ma and Mb cells. *Vision Res* **36**, 3901–3911.

Denk W & Detwiler PB (1999). Optical recording of light-evoked calcium signals in the functionally intact retina. *Proc Natl Acad Sci U S A* **96**, 7035–7040.

Fellin T, Pascual O, Gobbo S, Pozzan T, Haydon PG & Carmignoto G (2004). Neuronal synchrony mediated by astrocytic glutamate through activation of extrasynaptic NMDA receptors. *Neuron* **43**, 729–743.

Fiacco TA & McCarthy KD (2004). Intracellular astrocyte calcium waves *in situ* increase the frequency of spontaneous AMPA receptor currents in CA1 pyramidal neurons. *J Neurosci* **24**, 722–732.

Fields RD & Stevens-Graham B (2002). New insights into neuron-glia communication. *Science* **298**, 556–562.

Gilland E, Miller AL, Karplus E, Baker R & Webb SE (1999). Imaging of multicellular large-scale rhythmic calcium waves during zebrafish gastrulation. *Proc Natl Acad Sci U SA* **96**, 157–161.

Grosche J, Matyash V, Moller T, Verkhratsky A, Reichenbach A & Kettenmann H (1999). Microdomains for neuron–glia interaction: parallel fiber signaling to Bergmann glial cells. *Nat Neurosci* **2**, 139–143.

Guthrie PB, Knappenberger J, Segal M, Bennett MVL, Charles AC & Kater S (1999). ATP released from astrocytes mediates glial calcium waves. *J Neurosci* **19**, 520–528.

Haydon PG (2001). Glia: listening and talking to the synapse. *Nat Rev Neurosci* **2**, 185–193.

Hirase H, Qian L, Bartho P & Buzaki G (2004). Calcium dynamics of cortical astrocytic networks in vivo. *PLoS Biol* **2**, 494–499.

Ikegaya Y, Aaron G, Cossart R, Aronov D, Lampl I, Ferster D & Yuste R (2004). Synfire chains and cortical songs: temporal modules of cortical activity. *Science* **304**, 559–564.

Ikegaya Y, Le Bon-Jego M & Yuste R (2005). Large-scale imaging of cortical network activity with calcium indicators. *Neurosci Res* **52**, 132–138.

Lagnado MM & Baylor DA (1995). Concerted signaling by retinal ganglion cells. *Science* **270**, 1207–1210.

Makino CL & Dodd RL (1996). Multiple visual pigments in a photoreceptor of the salamander retina. *J Gen Physiol* **108**, 27–34.

Meister M, Lagnado L & Baylor DA (1995). Concerted signaling by retinal ganglion cells. *Science* **270**, 1207–1210.

Metea MR & Newman EA (2006). Calcium signaling in specialized glial cells. *Glia* **54**, 650–655.

Neuenschwander S, Castelo-Branco M & Singer W (1999). Synchronous oscillations in the cat retina. *Vision Res* **39**, 2485–2497.

Neuenschwander S & Singer W (1996). Long-range synchronization of oscillatory light responses in the cat retina and lateral geniculate nucleus. *Nature* **379**, 728–732.

Newman EA (2001). Propagation of intercellular calcium waves in retinal astrocytes and Müller cells. *J Neurosci* **21**, 2215–2223.

Newman EA (2003). Glial cell inhibition of neurons by release of ATP. *J Neurosci* **23**, 1659–1666.

Newman EA (2005). Calcium increases in retinal glial cells evoked by light-induced neuronal activity. *J Neurosci* **25**, 5502–5510.

Newman EA & Reichenbach A (1996). The Muller cell: a functional element of the retina. *Trends Neurosci* **19**, 307–312.

Newman EA & Zahs KR (1997). Calcium waves in retinal glial cells. *Science* **275**, 844–847.

Newman EA & Zahs KR (1998). Modulation of neuronal activity by glial cells in the retina. *J Neurosci* **18**, 4022–4028.

Parpura V, Basarsky TA, Liu F, Jeftinija K, Jeftinija S & Haydon PG (1994). Glutamate-mediated astrocyte-neuron signalling. *Nature* **369**, 744–747.

Parri HR, Gould TM & Crunelli V (2001). Spontaneous astrocytic Ca^{2+} oscillations *in situ* drive NMDA-mediated neuronal excitation. *Nat Neurosci* **4**, 803–812.

Pascual O, Casper KB, Kubera C, Zhang J, Revilla-Sanchez R, Sul JY, Takano H, Moss SJ, McCarthy K & Haydon PG (2005). Astrocytic purinergic signalling coordinates synaptic networks. *Science* **310**, 113–116.

Perea G & Araque A (2005*a*). Glial calcium signaling and neuron-glia communication. *Cell Calcium* **38**, 375–382.

Perea G & Araque A (2005*b*). Properties of synaptically evoked astrocyte calcium signal reveal synaptic information processing by astrocytes. *J Neurosci* **25**, 2192–2203.

Platel JC, Boisseau S, Dupuis A, Brocard J, Poupard A, Savasta M, Villaz M & Albrieux M (2005). Na^{+} channel-mediated Ca^{2+} entry leads to glutamate secretion in mouse neocortical preplate. *Proc Natl Acad Sci U S A* **102**, 19174–19179.

Platel JC, Dupuis A, Boisseau S, Villaz M, Albrieux M & Brocard J (2007). Synchrony of spontaneous calcium activity in mouse neocortex before synaptogenesis. *Eur J Neurosci* **25**, 920–928.

Reidel B, Orisme W, Goldmann T, Smith WC & Wolfrum U (2006). Photoreceptor vitality in organotypic cultures of mature vertebrate retinas validated by light-dependent molecular movements. *Vision Res* **46**, 4464–4471.

Ribelayga C & Mangel SC (2005). A circadian clock and light/dark adaptation differentially regulate adenosine in the mammal. *J Neurosci* **25**, 215–222.

Ribelayga C, Wang Y & Mangel SC (2004). A circadian clock in the fish retina regulates dopamine release via activation of melatonin receptors. *J Physiol* **554**, 467–482.

Rizzuto T & Pozzan T (2006). Microdomains of intracellular Ca^{2+}: molecular determinants and functional consequences. *Physiol Rev* **86**, 369–408.

Rogers KL, Stinnakre J, Agulhon C, Jublot D, Shorte SL, Kremer EJ & Brulet P (2005). Visualization of local Ca^{2+} dynamics with genetically encoded bioluminescent reporters. *Eur J Neurosci* **21**, 597–610.

Schell MJ, Molliver ME & Snyder SH (1995). D-Serine, an endogenous synaptic modulator: localization to astrocytes and glutamate-stimulated release. *Proc Natl Acad Sci U S A* **92**, 3948–3952.

Stella SL Jr, Bryson EJ, Cadetti L & Thoreson WB (2003). Endogenous adenosine reduces glutamatergic output from rods through activation of A_2-like adenosine receptors. *J Neurophysiol* **90**, 165–174.

Vallazza-Deschamps G, Cia D, Gong J, Jellali A, Duboc A, Forster V, Sahel JA, Tessier LH & Picaud S (2005). Excessive activation of cyclic nucleotide-gated channels contributes to neuronal degeneration of photoreceptors. *Eur J Neurosci* **22**, 1013–1022.

Volterra A & Meldolesi J (2005). Astrocytes, from brain glue to communication elements: the revolution continues. *Nat Rev Neurosci* **6**, 626–640.

Wang Y & Mangel SC (1996). A circadian clock regulates rod and cone input to fish retinal cone horizontal cells. *Proc Natl Acad Sci U S A* **93**, 4655–4660.

Webb SE, Lee KW, Karplus E & Miller AL (1997). Localized calcium transients accompany furrow positioning, propagation, and deepening during the early cleavage period of zebrafish embryos. *Dev Biol* **192**, 78–92.

Acknowledgements

We thank E. Kremer for providing Ad5-GA, and the Imaging Center of the Pasteur Institute for technical advice and the use of imaging equipment. We greatly thank C. Betancur, T. A. Fiacco and S. Gautron for critical reading of the manuscript. This work was supported by European Community (CE) and Pasteur Institute fellowships to C.A., by grants from the Pasteur Institute, the CNRS and the CE to P.B., and by grants to S.P. from the Fondation Ophtalmologique A. de Rothschild, the CE (EVI-GENORET-512036), Agence Nationale pour la Recherche (ANR GLAUCOME), and Agence Nationale pour la Recherche. J.-C.P. was supported by an Emergence fellowship from the Région Rhône-Alpes. J.B. was supported by an Action Concertée Incitative 'Jeunes Chercheurs' from the Ministère de l'Education Supérieure et de la Recherche.

Author's present address

J.-C. Platel: Departments of Neurosurgery and Cellular and Molecular Physiology, Yale University, New Haven, CT 06520-8082, USA.

Supplemental material

Online supplemental material for this paper can be accessed at:
http://jp.physoc.org/cgi/content/full/jphysiol.2007.135715/DC1

and

http://www.blackwell-synergy.com/doi/suppl/10.1113/jphysiol.2007.135715